



## FULL PAPER

# Transition metal complexes of Schiff base ligand based on 4,6-diacetyl resorcinol

Walaa H. Mahmoud<sup>1</sup> | M.M. Omar<sup>1</sup> | Yasmin M. Ahmed<sup>1</sup> |  
Gehad G. Mohamed<sup>1,2</sup>

<sup>1</sup>Chemistry Department, Faculty of Science, Cairo University, Giza, 12613, Egypt

<sup>2</sup>Egypt Nanotechnology Center, Cairo University, El-Sheikh Zayed, 6<sup>th</sup> October, 12588, Egypt

**Correspondence**

Gehad G. Mohamed, Chemistry Department, Faculty of Science, Cairo University, Giza, 12613, Egypt.  
Email: ggenidymohamed@sci.cu.edu.eg

Novel Schiff base ligand based on the condensation of 4,6-diacetyl resorcinol with 2-amino-4-methylthiazole in addition to its metal complexes with Cr (III), Mn (II), Fe (III), Co (II), Ni (II), Cu (II), Zn (II) and Cd (II) ions have been synthesized. The structure, electronic properties, and thermal behaviour of Schiff base and its metal complexes have been studied by elemental analysis, mass, <sup>1</sup>H NMR, IR spectra, thermal analysis, and theoretically by density function theory. The ligand acted as mononegative bidentate (NO) ligand and all complexes showed octahedral geometry except Cu (II) showed tetrahedral geometry as indicated from the spectral and magnetic studies. The Cu (II), Zn (II) and Cd (II) complexes were non electrolytes while the rest of the complexes were electrolytes. The antibacterial plus anticancer activities of the parent Schiff base and its metal complexes were screened. In addition, the molecular docking study was performed to explore the possible ways for binding to Crystal Structure of *Human Astrovirus capsid protein* (5ibv) receptor.

**KEYWORDS**

antibacterial and anticancer activity, density function theory, molecular docking, Schiff Base

## 1 | INTRODUCTION

Coordination chemistry of studying the transition metal complexes of Schiff bases has been enhanced by the current advancements in the subjects of medicine and bioinorganic chemistry.<sup>[1]</sup> Schiff bases as the condensation result of an amine and ketone or aldehyde with a general formula of R<sub>2</sub>C=NR are well-known organic compounds. Up to now, a broad range of Schiff bases has been made and used as ligands to prepare coordination compounds.<sup>[2]</sup>

A lot of researchers had studied the metal complexes of Schiff base ligands including one aromatic ring. Metal complexes of Schiff base ligands with two aromatic rings have been studied the lowest intense, while a new Schiff base ligands contain three aromatic rings were related by Binnemans et al., 2002.<sup>[3]</sup>

In fact, many metal complexes of sulfur-nitrogen chelating agents have been revealed to display approved cytotoxic (anticancer) activities. In the last twenty five years, a great deal of concern has been given to the study of metal complexes of sulfur ligands. Structural characterization and synthesis of this type of ligands are essential to ligands containing both hard and soft donor atoms may yield metal complexes with unusual magnetic properties and interesting stereochemistry and some of the ligands and their metal complexes are estimated to show biological activity.<sup>[4]</sup> This work targeted to synthesis new Schiff base and its metal complex. Different characterization tools were used for identification of the structures of the prepared compounds. The in vitro antibacterial and anti-breast cancer activities had also been screened. The possible binding of the prepared compounds with

Crystal Structure of Human Astrovirus capsid protein (5ibv) receptor was demonstrated.

## 2 | EXPERIMENTAL

All chemicals used were of the analytical reagent grade (AR) and of the maximum purity available. The chemicals used entered 2-amino-4-methylthiazole which was provided from Strems Chemical Inc., 4,6-diacetyl resorcinol (Sigma-Aldrich),  $\text{CrCl}_3 \cdot 6\text{H}_2\text{O}$ ,  $\text{MnCl}_2 \cdot 2\text{H}_2\text{O}$  and  $\text{FeCl}_3 \cdot 6\text{H}_2\text{O}$  (Sigma-Aldrich, Germany),  $\text{NiCl}_2 \cdot 6\text{H}_2\text{O}$ ,  $\text{CoCl}_2 \cdot 6\text{H}_2\text{O}$ ,  $\text{CuCl}_2 \cdot 2\text{H}_2\text{O}$  and  $\text{ZnCl}_2$  (BDH) and  $\text{CdCl}_2$  (Merck, Germany). Solvents of organic used were ethyl alcohol (95%), methyl alcohol and N,N-dimethylformamide (DMF). Deionized water was commonly consumed in all preparations.

### 2.1 | Solutions

Stock solutions of the Schiff base ligand ( $\text{H}_2\text{L}$ ) and its metal complex of  $1 \times 10^{-3}$  M was prepared by dissolving an exactly weighed amount in DMF. The conductivity, in that case measured for the metal complexes solutions. Dilute solutions of the Schiff base ligand and its metal complexes ( $1 \times 10^{-4}$  M) were prepared by exact dilution from the before and prepared stock solutions for measuring their UV-Vis spectra.

### 2.2 | Solution of anticancer study

A fresh stock solution ( $1 \times 10^{-3}$  M) of Schiff base ligand ( $0.12 \times 10^{-2}$  g  $\text{L}^{-1}$ ) was prepared in the suitable volume of DMF (90%). DMSO was used in cryopreservation of cells. RPMI-1640 medium was used. The medium was used for culturing and keep of the human tumor cell line. The medium was contributed in a powder form. It was gotten ready as follows: 10.4 g of medium was weighed, mixed with 2 g of sodium bicarbonate, completed to 1 l with distilled water and shaken prudently until complete dissolution. The medium was then uncontaminated by filtration in a Millipore bacterial filter (0.22 ml). The prepared medium was kept in a refrigerator ( $4^\circ\text{C}$ ) and checked at methodical intervals for contamination. Before use, the medium was warmed at  $37^\circ\text{C}$  in a water bath and supplemented with penicillin-streptomycin and FBS. Sodium bicarbonate was used for the preparation of RPMI-1640 medium. Isotonic trypan blue solution (0.05%) was prepared in normal saline and were used for feasibility counting. FBS (10%, heat inactivated at

$56^\circ\text{C}$  for 30 min), 100 units/mL penicillin and 2 mg/ml streptomycin were used for the supplementation of RPMI-1640 medium prior to use. Trypsin (0.25  $\times 10^{-1}\%$  w/v) was used for the picking of cells. Acetic acid (1% v/v) was used for dissolving unbound SRB dye. SRB (0.40%) dissolved in 1% acetic acid was used as a protein dye. A stock solution of trichloroacetic acid (50%) was prepared and stored. An amount of 50  $\mu\text{L}$  of the stock was added to 200  $\mu\text{L}$  of RPMI-1640 medium per well to yield a final concentration of 10% used for protein precipitation. Isopropanol (100%) and ethanol (70%) were used. Tris base (10 mM; pH =10.50) was used for SRB dye solubilization. Tris base (121.10 g) was dissolved in 1000 ml of distilled water and the pH was attuned using hydrochloric acid (2 M).

### 2.3 | Instrumentation

Microanalyses of carbon, hydrogen and nitrogen were carried out at the Microanalytical Center, Cairo University, Egypt, using a CHNS-932 (LECO) Vario elemental analyzer. Analyses of the metals were performed by dissolving the solid complexes in concentrated  $\text{HNO}_3$ , and dissolving the remainder in deionized water. The metal content was carried out using inductively coupled plasma atomic absorption spectrometry (ICP-AES), Egyptian Petroleum Research Institute. Fourier transform infrared (FT-IR) spectra were recorded with a Perkin-Elmer 1650 spectrometer ( $400\text{--}4000\text{ cm}^{-1}$ ) in KBr pellets.  $^1\text{H}$  NMR spectra, as solutions in  $\text{DMSO-}d_6$ , were chronicled with a 300 MHz Varian-Oxford Mercury at room temperature using tetra-methylsilane as an interior standard. Mass spectra were chronicled using the electron ionization technique at 70 eV with an MS-5988 GS-MS Hewlett-Packard instrument at the Microanalytical Center, National Center for Research, Egypt. UV-visible spectra were acquired with a Shimadzu UVmini-1240 spectrophotometer. Molar conductivities of  $10^{-3}$  M solutions of the solid complexes in DMF were measured with a Jenway 4010 conductivity meter. Thermogravimetric (TG) and differential thermogravimetric (DTG) analyses of the solid complexes were carried out from room temperature to  $1000^\circ\text{C}$  using a Shimadzu TG-50H thermal analyzer. Antimicrobial measurements were carried out at the Microanalytical Center, Cairo University, Egypt. Anticancer activity experiments were performed at the National Cancer Institute, Cancer Biology Department, Pharmacology Department, Cairo University. The optical density (OD) of each in good form was measured spectrophotometrically at 564 nm with an ELIZA microplate reader (Meter tech. R960, Lewiston, USA).

## 2.4 | Synthesis of Schiff base ligand

The symmetric Schiff base ligand ( $H_2L$ ) was synthesized by condensation of 4,6-diacetylresorcinol (4,6-DAR) in addition to 2-amino-4-methylthiazole. A solution of 2-amino-4-methylthiazole (15.4 mmol, 1.76 g) dissolved in ethanol was added dropwise to 4,6-DAR (15.4 mmol, 3 g) dissolved in DMF. The resulting mixture was stirred under reflux for about 4–5 hr at 100–150 °C, during which brown solid compound was separated. It was filtered, washed, recrystallized from diethyl ether and desiccated in vacuum (Scheme 1).

$H_2L$

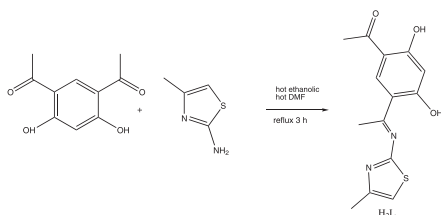
Yield 90%; m.p. 161 °C; orange solid. Anal. Calcd for  $C_{14}H_{14}N_2O_3S$  (%): C, 57.86; H, 4.82; N, 8.27; Found (%): C, 56.59; H, 4.39; N, 8.19. FT-IR ( $cm^{-1}$ ): phenolic  $\nu$  (OH) 3421, azomethine  $\nu$ (C=N) 1588, carbonyl (C=O) 1650.  $^1H$  NMR (300 MHz, DMSO- $d_6$ ,  $\delta$ , ppm): 8.41 (s, 1H, Ar-H (thiazole)), 6.38, 6.06 (s, 2H (benzene)), 12.72 (s, 1H, OH<sub>b</sub>), 10.00 (s, 1H, OH<sub>a</sub>),  $\lambda_{max}$  (nm): 248 ( $\pi$ - $\pi^*$ ), 321 (n- $\pi^*$ ).

## 2.5 | Synthesis of metal complexes

Complexes of  $H_2L$  in addition to Cr (III), Mn (II), Fe (III), Co (II), Ni (II), Cu (II), Zn (II) and Cd (II) metal ions were prepared by the reaction of 1:1 molar mixture of hot ethanolic solution (60 °C) of the suitable metal chloride (0.76 mmol) and  $H_2L$  (0.3 g, 0.76 mmol). The resulting mixture was stirred under reflux for 1 hr whereupon the complexes precipitated. They were collected by filtration and purified by washing several times with diethyl ether.

### 2.5.1 | [Cr (HL)(H<sub>2</sub>O)<sub>3</sub>Cl]Cl<sub>4</sub>H<sub>2</sub>O

Yield 84%; m.p. >300 °C; yellow solid. Anal. Calcd for  $C_{14}H_{27}Cl_2CrN_2O_{10}S$  (%): C, 31.21; H, 5.02; N, 5.20; Cr, 9.66. Found (%): C, 31.18; H, 4.84; N, 4.92; Cr, 9.29. FT-IR ( $cm^{-1}$ ):  $\nu$  (OH) 3428, azomethine  $\nu$ (C=N) 1532, carbonyl (C=O) 1632,  $\nu$ (H<sub>2</sub>O) stretching bands of coordinated water 967 and 835,  $\nu$ (M-O) 575 and  $\nu$ (M-N) 490.  $\lambda_{max}$



**SCHEME 1** Synthesis of Schiff base ligand

(nm): 252 ( $\pi$ - $\pi^*$ ), 311 (n- $\pi^*$ ).  $u_{eff}$ : 4.1;  $\Lambda_m$  ( $\Omega^{-1} mol^{-1} cm^2$ ) 60.7

### 2.5.2 | [Mn (HL)(H<sub>2</sub>O)<sub>4</sub>]Cl<sub>2</sub>H<sub>2</sub>O

Yield 86%; m.p. 180 °C; yellow solid. Anal. Calcd for  $C_{14}H_{25}ClMnN_2O_9S$  (%): C, 34.44; H, 5.12; N, 5.74; Mn, 11.27. Found (%): C, 34.28; H, 4.99; N, 5.60; Mn, 11.19. FT-IR ( $cm^{-1}$ ):  $\nu$  (OH) 3434, azomethine  $\nu$ (C=N) 1574, carbonyl (C=O) 1630,  $\nu$ (H<sub>2</sub>O) stretching bands of coordinated water 951 and 897,  $\nu$ (M-O) 579 and  $\nu$ (M-N) 480.  $\lambda_{max}$  (nm): 226 and 252 ( $\pi$ - $\pi^*$ ), 321 (n- $\pi^*$ ).  $u_{eff}$ : 5.22;  $\Lambda_m$  ( $\Omega^{-1} mol^{-1} cm^2$ ) 56.5.

### 2.5.3 | [Fe (HL)(H<sub>2</sub>O)<sub>4</sub>]Cl<sub>2</sub>·H<sub>2</sub>O

Yield 85%; m.p. 122 °C; orange solid. Anal. Calcd for  $C_{14}H_{23}Cl_2FeN_2O_8S$  (%): C, 33.18; H, 4.54; N, 5.53; Fe, 11.06. Found (%): C, 32.77; H, 4.49; N, 5.19; Fe, 10.86. FT-IR ( $cm^{-1}$ ):  $\nu$  (OH) 3429, azomethine  $\nu$ (C=N) 1534, carbonyl (C=O) 1635,  $\nu$ (H<sub>2</sub>O) stretching bands of coordinated water 940 and 839,  $\nu$ (M-O) 576 and  $\nu$ (M-N) 488.  $\lambda_{max}$  (nm): 252 ( $\pi$ - $\pi^*$ ), 320 (n- $\pi^*$ ).  $u_{eff}$ : 5.19;  $\Lambda_m$  ( $\Omega^{-1} mol^{-1} cm^2$ ) 105.9.

### 2.5.4 | [Co (HL)(H<sub>2</sub>O)<sub>4</sub>]Cl<sub>2</sub>·5H<sub>2</sub>O

Yield 84%; m.p. >300 °C; Greenish yellow solid. Anal. Calcd for  $C_{14}H_{31}ClCoN_2O_{12}S$  (%): C, 30.78; H, 5.68; N, 5.13; Co, 10.81. Found (%): C, 30.45; H, 5.40; N, 4.89; Co, 10.29. FT-IR ( $cm^{-1}$ ):  $\nu$  (OH) 3401, azomethine  $\nu$ (C=N) 1560, carbonyl (C=O) 1636,  $\nu$ (H<sub>2</sub>O) stretching bands of coordinated water 951 and 838,  $\nu$ (M-O) 577 and  $\nu$ (M-N) 498.  $\lambda_{max}$  (nm): 251 ( $\pi$ - $\pi^*$ ), 320 (n- $\pi^*$ ).  $u_{eff}$ : 4.78;  $\Lambda_m$  ( $\Omega^{-1} mol^{-1} cm^2$ ) 52.5.

### 2.5.5 | [Ni (HL)(H<sub>2</sub>O)<sub>4</sub>]Cl<sub>2</sub>·3H<sub>2</sub>O

Yield 80%; m.p. 240 °C; yellow solid. Anal. Calcd for  $C_{14}H_{27}ClNiN_2O_{10}S$  (%): C, 32.95; H, 5.30; N, 5.49; Ni, 12.57. Found (%): C, 32.81; H, 5.07; N, 5.33; Ni, 12.01. FT-IR ( $cm^{-1}$ ):  $\nu$  (OH) 3423, azomethine  $\nu$ (C=N) 1531, carbonyl (C=O) 1625,  $\nu$ (H<sub>2</sub>O) stretching bands of coordinated water 952 and 838,  $\nu$ (M-O) 579 and  $\nu$ (M-N) 450.  $\lambda_{max}$  (nm): 221 and 252 ( $\pi$ - $\pi^*$ ), 320 (n- $\pi^*$ ).  $u_{eff}$ : 3.17;  $\Lambda_m$  ( $\Omega^{-1} mol^{-1} cm^2$ ) 53.

### 2.5.6 | [Cu (HL)(H<sub>2</sub>O)Cl]·H<sub>2</sub>O

Yield 84%; m.p. 169 °C; brown solid. Anal. Calcd for  $C_{14}H_{17}ClCuN_2O_5S$  (%): C, 39.59; H, 4.01; N, 6.60; Cu, 14.96. Found (%): C, 39.27; H, 3.73; N, 6.22; Cu, 14.18.

FT-IR ( $\text{cm}^{-1}$ ):  $\nu$  (OH) 3407, azomethine  $\nu$ (C=N) 1567, carbonyl (C=O) 1631.  $\nu$ (H<sub>2</sub>O) stretching bands of coordinated water 945 and 837,  $\nu$ (M-O) 575 and  $\nu$ (M-N) 489.  $\lambda_{\text{max}}$  (nm): 226, 252  $\pi$ - $\pi^*$ , 319 n- $\pi^*$ .  $\mu_{\text{eff}}$ : 1.79;  $\Lambda_{\text{m}}$  ( $\Omega^{-1} \text{mol}^{-1} \text{cm}^2$ ) 50.2.

### 2.5.7 | [Zn (HL)(H<sub>2</sub>O)<sub>3</sub>Cl].3H<sub>2</sub>O

Yield 83%; m.p. 167 °C; yellow solid. Anal. Calcd for C<sub>14</sub>H<sub>25</sub>ClZnN<sub>2</sub>O<sub>9</sub>S (%): C, 33.74; H, 5.02; N, 5.62; Zn, 13.06. Found (%): C, 33.63; H, 4.48; N, 5.40; Zn, 12.87. FT-IR ( $\text{cm}^{-1}$ ):  $\nu$  (OH) 3400, azomethine  $\nu$ (C=N) disappeared, carbonyl (C=O) 1620,  $\nu$ (H<sub>2</sub>O) stretching bands of coordinated water 950 and 837,  $\nu$ (M-O) 573 and  $\nu$ (M-N) 470. <sup>1</sup>H NMR (300 MHz, DMSO-d<sub>6</sub>,  $\delta$ , ppm): 8.39 (s, 1H, Ar-H (thiazole)), 6.15, 6.35 (s, 2H (benzene)), 12.80 (s, 1H, OH<sub>b</sub>), disappeared (s, 1H, OH<sub>a</sub>),  $\lambda_{\text{max}}$  (nm): 245  $\pi$ - $\pi^*$ , 321 n- $\pi^*$ .  $\mu_{\text{eff}}$ : diamagnetic;  $\Lambda_{\text{m}}$  ( $\Omega^{-1} \text{mol}^{-1} \text{cm}^2$ ) 19.5.

### 2.5.8 | [CdR(HL)(H<sub>2</sub>O)<sub>3</sub>Cl]

Yield 85%; m.p. >300 °C; yellow solid. Anal. Calcd for C<sub>14</sub>H<sub>19</sub>ClCdN<sub>2</sub>O<sub>6</sub>S (%): C, 34.20; H, 3.87; N, 5.70; Cd, 22.88. Found (%): C, 33.85; H, 3.41; N, 5.31; Cd, 22.59. FT-IR ( $\text{cm}^{-1}$ ):  $\nu$  (OH) 3396, azomethine  $\nu$ (C=N) 1567, carbonyl (C=O) 1634,  $\nu$ (H<sub>2</sub>O) 958 and 836,  $\nu$ (M-O) 578,  $\nu$ (M-N) 490. <sup>1</sup>H NMR (300 MHz, DMSO-d<sub>6</sub>,  $\delta$ , ppm): 8.40 (s, 1H, Ar-H (thiazole)), 6.07, 6.34 (s, 2H (benzene)), 12.80 (s, 1H, OH<sub>b</sub>), disappeared (s, 1H, OH<sub>a</sub>),  $\lambda_{\text{max}}$  (nm): 258  $\pi$ - $\pi^*$ , 321 n- $\pi^*$ .  $\mu_{\text{eff}}$ : diamagnetic;  $\Lambda_{\text{m}}$  ( $\Omega^{-1} \text{mol}^{-1} \text{cm}^2$ ) 7.

## 2.6 | Spectrophotometric studies

The absorption spectra were recorded for  $1 \times 10^{-5}$  M solutions of the Schiff base ligand and its metal complexes in DMF, except for Cr (III) complex that had a concentration of  $5 \times 10^{-4}$  M and Cd (II), Co (II), Zn (II) complexes that had a concentration of  $10^{-4}$  M. The spectra were scanned within the wavelength range from 200 to 700 nm.

## 2.7 | Pharmacology

### 2.7.1 | Antibacterial activities

Antimicrobial activity of the tested samples was determined by a modified Kirby-Bauer disc diffusion

method.<sup>[5]</sup> Briefly, 100  $\mu$ l of the test bacteria were grown in 10 ml of fresh media until they reached a count of approximately 108 cells/ml for bacteria.<sup>[6]</sup> 100  $\mu$ l of microbial suspension was spread onto agar plates corresponding to the broth in which they were maintained. Isolated colonies of each organism that may be playing a pathogenic part should be selected from primary agar plates and tested for susceptibility by disc diffusion method.<sup>[7]</sup> Plates inoculated Gram(+) bacteria as *Staphylococcus aureus* and *Bacillus subtilis* and Gram(-) bacteria as *Escherichia coli* and *Pseudomonas aeruginosa*. They were incubated at 35–37 °C for 24–48 hr and then the diameters of the inhibition zones were calculated in millimeters.<sup>[5]</sup> Standard discs of amikacin (antibacterial agent), served as positive controls for antimicrobial activity but filter discs impregnated with 10  $\mu$ l of solvent (distilled water, chloroform, DMSO) were used as a negative control. Blank paper disks (Schleicher & Schuell, Satis Lda, Spain) with a diameter of 8.0 mm were impregnated with 10  $\mu$ l of tested concentration of the stock solutions (20 mg/ml).

When a filter paper disc impregnated with a tested chemical is placed on agar, the chemical will diffuse from the disc into the agar. This diffusion will place the chemical in the agar only around the disc. The solubility of the chemical and its molecular size will determine the size of the area of chemical infiltration around the disc. If an organism is placed on the agar it will not grow in the area around the disc if it is susceptible to the chemical. This area of no growth around the disc is known as a zone of inhibition or Clear zone. For the disc diffusion, the zone diameters were measured with slipping calipers of the National Committee for Clinical Laboratory Standards. Agar-based methods such as E-test and disk diffusion can be good alternatives because they are easier and more rapidly than broth-based methods.<sup>[8,9]</sup> All experiments were performed as triplicate and the data plotted where the mean value.<sup>[10]</sup>

### 2.7.2 | Anticancer activity

Potential cytotoxicity of the compounds was tested via the method of Skehan and Storeng.<sup>[11]</sup> Cells were plated in 96-multiwell plate (104 cells/well) for 24 hr before treatment using the compounds to let attachment of cell to the wall of the plate altered concentrations of the compounds under investigation (0, 5, 12.5, 25, 50 and 100  $\mu$ g/ml) were added to the cell monolayer and triplicate wells were prepared for each individual dose. The monolayer cells were kept warm with the compounds for 48 hr at 37 °C and in 5% CO<sub>2</sub> atmosphere. After 48 hr, cells were immobile, washed and stained with SRB stain.

Excess stain was washed with acetic acid and attached stain was convalesced with tris-EDTA buffer. The optical density (O.D.) of each well was measured spectrophotometrically at 564 nm using an ELIZA microplate reader, the mean background absorbance was automatically subtracted and mean values of each drug concentration was calculated. The relation between drug concentration and surviving fraction is plotted to get the survival curve of breast tumor cell line for each compound.

The percentage of cell survival was calculated as follows:

$$\text{Survival fraction} = \frac{\text{O.D. (treated cells)}}{\text{O.D. (control cells)}}$$

The IC<sub>50</sub> values (the concentrations of the Schiff base ligand (L) or its metal complexes required to produce 50% inhibition of cell growth). The experiment was repeated 3 times.<sup>[11,12]</sup>

### 2.7.3 | Computational methodology

Gaussian03 suite of program was used for the electronic structure calculations for H<sub>2</sub>L and Cu (II) complex. DFT based B3LYP method along using the LANL2DZ basis set was employed for full optimization. So as to incorporate the effect of the solvent around the molecule, the TD-DFT method (along with LANL2DZ basic set) was used to calculate the electronic absorption spectra of the ligand and its Cu (II) complex. The contribution of molecular orbital on HOMO and LUMO were also calculated.

### 2.7.4 | Molecular docking

So as to find out the achievable binding modes of the best active compounds against the Crystal structure of Human Astrovirus capsid protein (PDB ID: 5IBV), molecular docking studies were performed with MOE2008 software. It is a rigid molecular docking software and is an interactive molecular graphics program in support of calculating and displaying feasible docking modes of a receptor and ligand and complex molecules. It requires the ligand and the receptor as input in PDB format. The amino acid chain was kept and the water molecules and co-crystallized ligands and chloride ions in out sphere were removed. The structure of ligand in PDB file format was created using Gaussian09 software. Crystal structure of Human Astrovirus capsid protein (PDB ID: 5IBV) was downloaded from the protein data bank (<http://www.rcsb.org/pdb>).

## 2.8 | Results and discussion

### 2.8.1 | Elemental analysis

The synthesized Schiff base ligand was an orange solid and stable at room temperature. It was soluble in ethanol and DMF. The results obtained were in good agreement using those calculated from the suggested formula (see experimental part). The structure of the Schiff base ligand under study was shown in Figure 1.

Metal complexes of H<sub>2</sub>L were synthesized. The metal/ligand ratio was found to be 1:1 in all complexes, which have been arrived by estimating the carbon, hydrogen, nitrogen and metal contents of the complexes. Its metal complexes had the composition of MHL type. The results of the experimental elemental analysis of H<sub>2</sub>L and its complexes had closely values to the theoretical calculations.<sup>[12]</sup>

### 2.8.2 | Mass spectra

The mass spectrum of H<sub>2</sub>L ligand exhibited a molecular ion peak at m/z = 290.24 amu corresponding to [M]<sup>+</sup>, which confirmed the proposed formula [C<sub>14</sub>H<sub>13</sub>N<sub>2</sub>O<sub>3</sub>S]<sup>+</sup> and in good agreement with the calculated value (290.36 amu). The intensity of the peaks as the results of fragmentation was given in Figure 2a.

The mass spectrum of Cu (II) complex revealed a molecular ion peak at m/z = 424.21 amu which was coextensive with the calculated weight of 424.36 amu. This result confirmed the stoichiometry of this complex as being of [MHL] type. On the other hand, the peak of the parent ligand in the mass spectrum of the Cu (II) complex seemed at m/z 290.97 amu (Figure 2b).

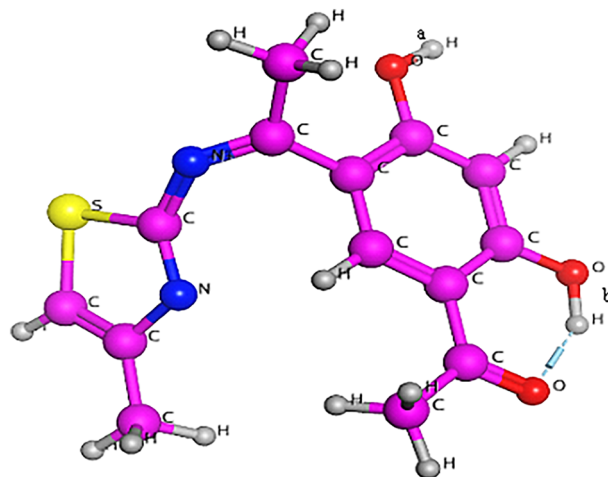
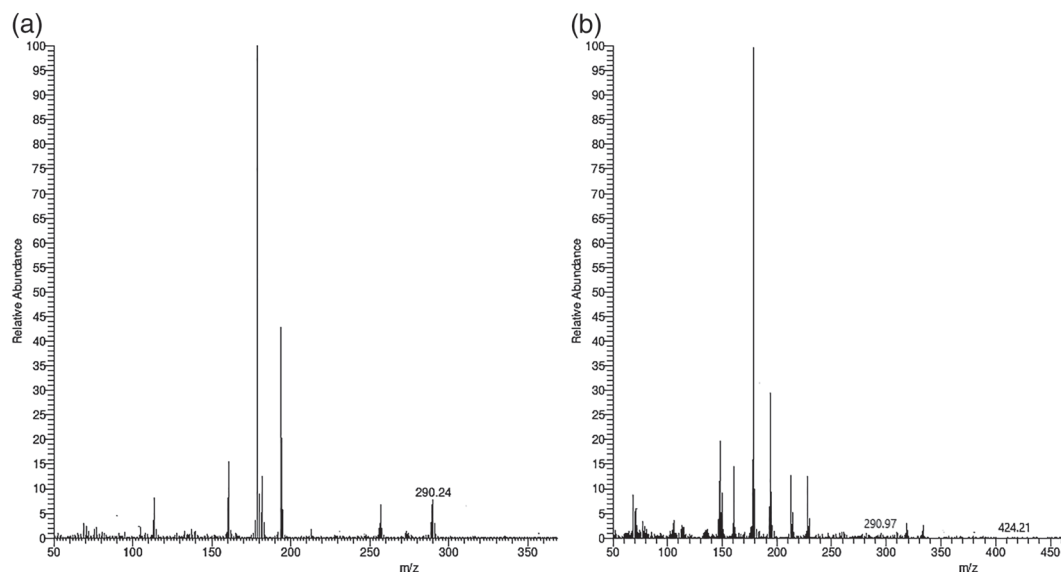


FIGURE 1 Structure of Schiff base ligand (H<sub>2</sub>L)



**FIGURE 2** Mass spectra of the (a) Schiff base ligand ( $H_2L$ ) and (b)  $[Cu(HL)Cl(H_2O)]H_2O$  complex

### 2.8.3 | FT-IR spectral study

The FT-IR spectrum of  $H_2L$  ligand showed a lack of the  $NH_2$  stretching band characteristic of 2-amino-4-methylthiazole. On the other hand, a new, strong and sharp vibration band appeared at  $1588\text{ cm}^{-1}$  due to the azomethine group ( $C=N$ ), demonstrating the formation of the Schiff base product ( $H_2L$ ). The band of keto carbonyl  $\nu(C=O)$  group appeared at  $1650\text{ cm}^{-1}$ . The  $\nu(OH)$  stretching frequencies of  $H_2L$  which lies at  $3421\text{ cm}^{-1}$  still persist even after the formation of the ligand.<sup>[13]</sup>

The FT-IR spectra of the complexes were compared with this free ligand to distinguish the coordination sites of chelation. The band of azomethine  $\nu(C=N)$  group was shifted to lower frequency in the spectra of all the complexes in the range  $1531\text{--}1567\text{ cm}^{-1}$ , showing the involvement of azomethine nitrogen in the chelation to the metal ions. The band of keto carbonyl  $\nu(C=O)$  group was slightly shifted to lower frequency in the spectra of all the complexes. The variance observed in these values may be due to expected H-bonding between the hydrogen atoms of the  $-OH_b$  group and the keto carbonyl oxygen.<sup>[14]</sup>

New bands for all complexes appeared in the region  $450\text{--}498\text{ cm}^{-1}$  attributed to  $\nu(M-N)$ . The bands in the region  $573\text{--}579\text{ cm}^{-1}$  in the spectra of all the complexes were assigned to  $\nu(M-O)$  stretching vibration of the binding of the ligand to the metal ions which was succeeded via coordination of metal ions with the deprotonated phenolic oxygen ( $-OH_a$ ). Also, OH stretching vibration band at  $3421\text{ cm}^{-1}$  in the free ligand appeared as broad band in the metal complexes. This can attributed to the

OH group and  $H_2O$  molecules in the complexes. This make it difficult to differentiate and hence  $^1H$  NMR was carried out to give us an idea about the OH which participated in binding to the metal ions. Two new  $\nu(H_2O)$  bands of coordinated water molecules appeared in the FT-IR spectra of the metal complexes at  $836\text{--}897$  and  $940\text{--}967\text{ cm}^{-1}$ , indicating the binding of water molecules to the metal ions. In consequence, the  $H_2L$  ligand acted as mononegative bidentate chelating agent, bonded to the metal ions via a nitrogen atom and deprotonated phenolic oxygen atom of the Schiff base.<sup>[15,16]</sup>

### 2.8.4 | $^1H$ NMR Spectrum

$^1H$  NMR spectral data ( $\delta$  ppm) of the free ligand in relation to TMS (0 ppm) in  $DMSO-d_6$  were obtained to approve the ligand structure and its purity. The signals observed at 10.00 and 12.72 ppm may be assigned to two phenolic  $OH_a$  and  $OH_b$  groups, respectively. The spectrum of free ligand ( $H_2L$ ) exhibited a signal at 8.41 ppm region, which may be assigned to thiazole protons (s, 1H). In the aromatic region, two singlet signals observed at 6.38 and 6.06 ppm (s, 2H, Ar-H).<sup>[17,18]</sup>

$^1H$  NMR spectral ( $\delta$  ppm) of Zn (II) and Cd (II) complexes showed phenolic  $-OH_b$  group at 12.80 ppm, which appeared in the same position of the free ligand. This confirmed its nonparticipation in chelate formation and this slight shift can assign to hydrogen bond formation with the adjacent carbonyl group. But the signal for  $OH_a$  was disappeared in the  $^1H$  NMR spectra of both Zn (II) and Cd (II) complexes. This indicated

that  $\text{OH}_a$  participated in coordination to the metal ions with proton displacement. In the aromatic region, two singlet signals were observed at 6.15 and 6.35 for Zn (II) complex and at 6.07 and 6.34 ppm for Cd (II) complex. On the other hand the thiazole proton still appear in the same position as free ligand.<sup>[12]</sup> The data of the  $^1\text{H}$  NMR spectra of Schiff base ligand ( $\text{H}_2\text{L}$ ) and its mononuclear metal complexes are given in the experimental part.

### 2.8.5 | Molar conductance measurements

The molar conductance values of the complexes were measured at room temperature and these data showed that Cu (II), Zn (II) and Cd (II) complexes have no conductance and they were considered as nonelectrolytes. Cr (III), Mn (II), Co (II) and Ni (II) complexes had molar conductivity values of 60.7, 56.5, 52.5 and  $53.0 \Omega^{-1} \text{mol}^{-1} \text{cm}^2$ , respectively. These data suggested that these complexes were ionic in nature and they were 1:1 electrolytes. The Fe (III) complex had a molar conductivity value of  $105.90 \Omega^{-1} \text{mol}^{-1} \text{cm}^2$ , which suggested that this complex was ionic in nature and it was a 1:2 electrolyte.<sup>[19,20]</sup>

### 2.8.6 | UV-vis absorption studies

It is probable to draw up the electronic transitions and foretell the geometry with the help of magnetic moments of most metal ions. The main absorption band of the ligand is at 248 and 321 nm and they were assigned to  $\pi \rightarrow \pi^*$  and  $n \rightarrow \pi^*$  transitions within the aromatic rings in the ligand, respectively. The bands in all metal complexes located at 221–258 nm and 311–321 nm region were assigned to  $\pi \rightarrow \pi^*$  and  $n \rightarrow \pi^*$  transitions, respectively, which can be related to the binding of these coordination centres to the central metal ions.<sup>[21]</sup>

### 2.8.7 | Electronic spectral study

The diffused reflectance spectra of the mononuclear complexes were carried out within the range 200–1000 nm. It is probable to draw up the electronic transitions and detect the geometry through the help of magnetic moments of most metal ions.

The electronic spectrum of Cr (III) complex showed three spins allowed bands at 19110, 23510 and  $25910 \text{ cm}^{-1}$ . These bands may be assigned to  $^4\text{A}_{2g}(\text{F}) \rightarrow ^4\text{T}_{2g}(\text{F})$ ,  $^4\text{A}_{2g}(\text{F}) \rightarrow ^4\text{T}_{1g}(\text{F})$  and  $^4\text{A}_{2g}(\text{F}) \rightarrow ^4\text{T}_{1g}(\text{P})$  transitions

suggesting the octahedral geometry of the complex. The magnetic moment was found to be 4.01 B.M. which confirmed octahedral geometry of Cr (III) complex.<sup>[22]</sup>

The Mn (II) complex showed three spins allowed bands at 18020, 22710 and  $26150 \text{ cm}^{-1}$ . These bands may be assigned to  $^4\text{T}_{1g} \rightarrow ^6\text{A}_{1g}$ ,  $^4\text{T}_{2g}(\text{G}) \rightarrow ^6\text{A}_{1g}$  and  $^4\text{T}_{1g}(\text{D}) \rightarrow ^6\text{A}_{1g}$  transitions suggesting the octahedral geometry of the complex. The magnetic moment was found to be 5.22 B.M. which confirmed octahedral geometry of Mn (II) complex.<sup>[22,23]</sup>

The Fe (III) complex showed three spins allowed bands at 21975, 20690 and  $17140 \text{ cm}^{-1}$ . These bands may be assigned to  $^4\text{T}_{2g}(\text{G}) \rightarrow ^6\text{A}_{1g}$ ,  $^4\text{T}_{2g}(\text{G}) \rightarrow ^6\text{A}_{1g}$  and  $^4\text{T}_{1g}(\text{D}) \rightarrow ^6\text{A}_{1g}$  transitions indicating the octahedral geometry of the complex. The magnetic moment was 5.19 B.M. which confirmed octahedral geometry of Fe (III) complex.

Cobalt (II) complex showed three spins allowed bands at 23120, 21010 and  $15985 \text{ cm}^{-1}$ . These bands may be assigned to  $^4\text{T}_{1g}(\text{F}) \rightarrow ^4\text{T}_{2g}(\text{F})$ ,  $^4\text{T}_{1g}(\text{F}) \rightarrow ^4\text{A}_{2g}(\text{F})$  and  $^4\text{T}_{1g}(\text{F}) \rightarrow ^4\text{T}_{2g}(\text{P})$  transitions suggesting the octahedral geometry of the complex. The magnetic moment is 4.78 B.M. which confirmed octahedral geometry of cobalt (II) complex.

The Ni (II) complex showed three spins allowed bands at 27870, 21985 and  $12110 \text{ cm}^{-1}$ . These bands may be assigned to  $^3\text{A}_{2g} \rightarrow ^3\text{T}_{1g}(\text{P})$ ,  $^3\text{T}_{1g}(\text{P}) \rightarrow ^3\text{A}_{2g}$  and  $^3\text{A}_{2g}(\text{F}) \rightarrow ^3\text{T}_{1g}(\text{F})$  transitions indicating the octahedral geometry of the complex. The magnetic moment was 3.17 B.M. which confirmed octahedral geometry of Ni (II) complex.<sup>[23–25]</sup>

The Cu (II) complex showed two spins allowed bands at assigned to  $^2\text{B}_{1g} \rightarrow ^2\text{A}_{1g}$  and  $^2\text{B}_{1g} \rightarrow ^2\text{B}_{2g}$  transitions. Also the magnetic moment value of the copper (II) complex is 1.30 B.M. This indicated the formation of tetrahedral geometry of the complex.<sup>[9,26]</sup>

The Zn (II) and Cd (II) complexes were diamagnetic. According to the empirical formulae, an octahedral geometry was suggested for the Zn (II) and Cd (II) complexes.

Thermal analysis.

TG and DTG analysis results of  $\text{H}_2\text{L}$  and its metal complexes at a heating rate of  $10 \text{ }^\circ\text{C}/\text{min}$  in nitrogen atmosphere over the range from ambient temperature to  $1000 \text{ }^\circ\text{C}$  were summarized in Table (1).

The Schiff base ligand with the molecular formula ( $\text{C}_{14}\text{H}_{14}\text{N}_2\text{O}_3\text{S}$ ) was thermally decomposed in two successive decomposition steps, within the range from 30 to  $900 \text{ }^\circ\text{C}$  via total mass loss of 98.69% (calcd. = 100%). The first and second stages within the temperature range of  $30\text{--}900 \text{ }^\circ\text{C}$  which correlated with evolution of  $\text{C}_{14}\text{H}_{14}\text{N}_2\text{O}_3\text{S}$  molecule with a maximum at 215 and  $388 \text{ }^\circ\text{C}$ .

**TABLE 1** Thermoanalytical results (TG and DTG) of Schiff base ligand (H<sub>2</sub>L) and its metal complexes

Complex	TG range (°C)	DTG <sub>max</sub> (°C)	n*	Mass loss Total mass loss Estim (calcd)%	Assignment	Residues
H <sub>2</sub> L	30–900	215,388	2	98.69(100) 98.69 (100)	-Loss of C <sub>14</sub> H <sub>14</sub> N <sub>2</sub> O <sub>3</sub> S.	
[Cr (HL)(H <sub>2</sub> O) <sub>3</sub> Cl]	30–100 100–220	50 170	1 1	9.48 (10.03) 19.73 (19.97) 44.48(44.67)	-Loss of 3H <sub>2</sub> O. -Loss of 1/2Cl <sub>2</sub> and 4H <sub>2</sub> O. -Loss of 1/2Cr <sub>2</sub> O <sub>3</sub> + 5C	
Cl.4H <sub>2</sub> O	220–900	458,825	2	73.69(74.67)	of 1/2Cl <sub>2</sub> and C <sub>9</sub> H <sub>13</sub> N <sub>2</sub> O <sub>1.5</sub> S.	
[Mn (HL)(H <sub>2</sub> O) <sub>4</sub> Cl.2H <sub>2</sub> O]	30–210 210–900	50,165 300,650	2 2	30.60 (29.41) 39.56(41.20) 70.16(70.61)	-Loss of 6H <sub>2</sub> O and 1/2Cl <sub>2</sub> . -Loss of C <sub>8</sub> H <sub>13</sub> N <sub>2</sub> O <sub>2</sub> S.	MnO +6C
[Fe (HL)(H <sub>2</sub> O) <sub>4</sub> ]Cl <sub>2</sub> .H <sub>2</sub> O	30–350 350–900	75,300 480,650	2 2	32.00(31.80) 38.10(38.11) 70.10 (69.91)	-Loss of 5H <sub>2</sub> O and Cl <sub>2</sub> . -Loss of C <sub>8</sub> H <sub>13</sub> N <sub>2</sub> O <sub>1.5</sub> S.	1/2Fe <sub>2</sub> O <sub>3</sub> + 6C
[Co (HL)(H <sub>2</sub> O) <sub>4</sub> ]Cl.5H <sub>2</sub> O	30–140 140–250	65,105 195	2 1	13.89 (13.19) 23.59 (22.99) 45.95(45.62)	-Loss of 4H <sub>2</sub> O. -Loss of 1/2Cl <sub>2</sub> and 5H <sub>2</sub> O. -Loss of C <sub>12</sub> H <sub>13</sub> N <sub>2</sub> O <sub>2</sub> S.	CoO + 2C
[Ni (HL)(H <sub>2</sub> O) <sub>4</sub> ]Cl.3H <sub>2</sub> O	250–900	520	1	83.43 (81.80)	-Loss of 2H <sub>2</sub> O. -Loss of 1/2Cl <sub>2</sub> , 5H <sub>2</sub> O and C <sub>14</sub> H <sub>13</sub> N <sub>2</sub> O <sub>2</sub> S	NiO
[Cu (HL)(H <sub>2</sub> O)Cl].H <sub>2</sub> O	30–100 100–900	75 190,420,500	1 3	7.61 (7.06) 78.00 (78.16) 85.61 (85.22)	-Loss of H <sub>2</sub> O. -Loss of H <sub>2</sub> O, 1/2Cl <sub>2</sub> and C <sub>11</sub> H <sub>13</sub> N <sub>2</sub> O <sub>2</sub> S.	CuO +3C
[Zn (HL)(H <sub>2</sub> O) <sub>3</sub> Cl].3H <sub>2</sub> O	30–110 110–900	80 210	1 1	3.98 (4.24) 68.13 (68.45) 72.11 (72.69)	-Loss of 2H <sub>2</sub> O. -Loss of 1/2Cl <sub>2</sub> , 4H <sub>2</sub> O and C <sub>14</sub> H <sub>13</sub> N <sub>2</sub> O <sub>2</sub> S.	ZnO
[Cd (HL)(H <sub>2</sub> O) <sub>3</sub> Cl]	30–100100-900	50 190,500	1 2	7.38 (7.23) 76.06 (76.43) 83.44 (83.66)	-Loss of 2H <sub>2</sub> O. -Loss of 1/2Cl <sub>2</sub> , 4H <sub>2</sub> O and C <sub>14</sub> H <sub>13</sub> N <sub>2</sub> O <sub>2</sub> S.	CdO
[Cd (HL)(H <sub>2</sub> O) <sub>3</sub> Cl]	30–900	200,750	2	73.25 (73.79) 73.25 (73.79)	-Loss of 1/2Cl <sub>2</sub> , 3H <sub>2</sub> O and C <sub>14</sub> H <sub>13</sub> N <sub>2</sub> O <sub>2</sub> S.	

n\* = number of decomposition step.

The [Cr (HL)(H<sub>2</sub>O)<sub>3</sub>Cl]Cl<sub>4</sub>H<sub>2</sub>O complex showed four decomposition stages within the range from 30 to 900 °C through total mass loss of 73.69% (calcd. = 74.67%) leaving ½Cr<sub>2</sub>O<sub>3</sub> contaminated by carbon atoms as residue. The first stage within the temperature range of 30–100 °C which correlated by evolution of three uncoordinated water molecules with mass loss of 9.48% (calculated mass loss = 10.03%) with a maximum at 50 °C. The second stage within the temperature range of 100–220 °C which correlated by evolution of four water molecules and ½ Cl<sub>2</sub> with mass loss of 19.73% (calculated mass loss = 19.97%) with maximum at 170 °C. The last two stages within the temperature range of 220–900 °C which correlated through evolution of ½ Cl<sub>2</sub> and C<sub>9</sub>H<sub>13</sub>N<sub>2</sub>O<sub>1.5</sub>S molecule with mass loss of 44.48% (calculated mass loss = 44.67%) with two maximum at 458 and 825 °C.

The [Mn (HL)(H<sub>2</sub>O)<sub>4</sub>Cl]Cl<sub>2</sub>H<sub>2</sub>O complex showed four decomposition stages within the range from 30 to 900 °C through total mass loss of 70.16% (calcd. = 70.61%) leaving MnO contaminated by carbon atoms as residue. The first and second stages within the temperature range of 30–210 °C which correlated by evolution of six water molecules and ½ Cl<sub>2</sub> with mass loss of 30.60% (calculated mass loss = 29.41%) with a maximum at 50 and 165 °C. The last two stages within the temperature range of 210–900 °C which correlated through evolution of C<sub>8</sub>H<sub>13</sub>N<sub>2</sub>O<sub>2</sub>S molecule with mass loss of 39.56% (calculated mass loss = 41.20%) with two maximum at 300 and 650 °C.

The [Fe (HL)(H<sub>2</sub>O)<sub>4</sub>]Cl<sub>2</sub>H<sub>2</sub>O complex showed four decomposition stages within the range from 30 to 900 °C with total mass loss of 70.10% (calcd. = 69.91%) leaving ½Fe<sub>2</sub>O<sub>3</sub> contaminated by carbon atoms as residue. The first and second stages within the temperature range of 30–350 °C which correlated through evolution of 5H<sub>2</sub>O and Cl<sub>2</sub> molecules by mass loss of 32.00% (calculated mass loss = 31.80%) with a maximum at 75 and 300 °C. The last two stages within the temperature range of 350–900 °C which correlated through evolution of C<sub>8</sub>H<sub>13</sub>N<sub>2</sub>O<sub>1.5</sub>S with mass loss of 38.10% (calculated mass loss = 38.11%) with two maximum at 480 and 650 °C.

The [Co (HL)(H<sub>2</sub>O)<sub>4</sub>]Cl<sub>2</sub>5H<sub>2</sub>O complex showed four decomposition stages within the range from 30 to 900 °C with total mass loss of 83.43% (calcd. = 81.80%) leaving CoO contaminated by carbon atoms as residue. The first and second stages within the temperature range of 30–140 °C which correlated through evolution of 4H<sub>2</sub>O uncoordinated molecules with mass loss of 13.89% (calculated mass loss = 13.19%) with a maximum at 65 and 105 °C. The third stage within the temperature range of 140–250 °C which correlated through evolution of 5H<sub>2</sub>O

and ½ Cl<sub>2</sub> molecules by mass loss of 23.59% (calculated mass loss = 22.99%) with a maximum at 195 °C. The last stage within the temperature range of 250–900 °C which correlated through evolution of C<sub>12</sub>H<sub>13</sub>N<sub>2</sub>O<sub>2</sub>S molecule with mass loss of 45.95% (calculated mass loss = 45.62%) with maximum at 520 °C.

The [Ni (HL)(H<sub>2</sub>O)<sub>4</sub>]Cl<sub>2</sub>3H<sub>2</sub>O complex showed four decomposition stages within the range from 30 to 900 °C with total mass loss of 85.61% (calcd. = 85.22%) leaving NiO as residue. The first stage within the temperature range of 30–100 °C which correlated through evolution of 2H<sub>2</sub>O uncoordinated molecules by mass loss of 7.61% (calculated mass loss = 7.06%) with a maximum at 75 °C. The last three stages within the temperature range of 100–900 °C which correlated through evolution of 5H<sub>2</sub>O, ½ Cl<sub>2</sub> and C<sub>14</sub>H<sub>13</sub>N<sub>2</sub>O<sub>2</sub>S molecules with mass loss of 78.00% (calculated mass loss = 78.16%) with a maximum at 190, 420 and 500 °C.

The [Cu (HL)(H<sub>2</sub>O)Cl]H<sub>2</sub>O complex showed two decomposition stages within the range from 30 to 900 °C with total mass loss of 72.11% (calcd. = 72.69%) leaving CuO and carbon atoms as residue. The first stage within the temperature range of 30–110 °C which correlated through evolution of H<sub>2</sub>O uncoordinated molecules with mass loss of 3.98% (calculated mass loss = 4.24%) with a maximum at 80 °C. The last stage within the temperature range of 110–900 °C which correlated through evolution of H<sub>2</sub>O, ½ Cl<sub>2</sub> and C<sub>11</sub>H<sub>13</sub>N<sub>2</sub>O<sub>2</sub>S molecules, by mass loss of 68.13% (calculated mass loss = 68.45%) with a maximum at 210 °C.

The [Zn (HL)(H<sub>2</sub>O)<sub>3</sub>Cl]3H<sub>2</sub>O complex showed three decomposition stages within the range from 30 to 900 °C with total mass loss of 83.44% (calcd. = 83.66%) leaving ZnO as residue. The first stage within the temperature range of 30–100 °C which correlated through evolution of 2H<sub>2</sub>O uncoordinated molecules with mass loss of 7.38% (calculated mass loss = 7.23%) with a maximum at 50 °C. The last two stages within the temperature range of 100–900 °C which correlated through evolution of 4H<sub>2</sub>O, ½ Cl<sub>2</sub> and C<sub>14</sub>H<sub>13</sub>N<sub>2</sub>O<sub>2</sub>S molecules by mass loss of 76.06% (calculated mass loss = 76.43%) with a maximum at 190 and 500 °C.

The [Cd (HL)(H<sub>2</sub>O)<sub>3</sub>Cl] complex showed two decomposition stages within the range from 30 to 900 °C with total mass loss of 73.25% (calcd. = 73.79%) leaving CdO as residue. Which correlated through evolution of 3H<sub>2</sub>O, ½ Cl<sub>2</sub> and C<sub>14</sub>H<sub>13</sub>N<sub>2</sub>O<sub>2</sub>S molecules with a maximum at 200 and 750 °C.

The thermogram of the complexes confirmed their structure where the presence of uncoordinated water molecules in all metal complexes except Cd (II) complex was suggested. and all complexes had octahedral geometry except Cu (II) complex tetrahedral geometry.

## 2.8.8 | Geometry optimization.

The completely optimized geometries of the ligand H<sub>2</sub>L and its Cu (II) complex were shown in Figure 3. The values of the certain bond lengths and bond angles calculated for Cu (II) complex showed distorted tetrahedral geometry around the Cu (II) ion (Table 2). A slight elongation in bond lengths C10-N1, N1-C27 and C2-O15 was noted in Cu (II) complex as ligand H<sub>2</sub>L coordinated through azomethine nitrogen and deprotonated phenolic oxygen. The Cu34-O15, Cu34-N1, Cu34-Cl35 and Cu34-O36 bond lengths were found to be 1.92, 1.99, 2.31 and 2.00 Å, respectively. The two positions were occupied by azomethine nitrogen and deprotonated phenolic oxygen however another two positions were occupied by chloride ion and oxygen water. The bond angles in the coordination sphere of Cu (II) complex were indicative of a distorted tetrahedral geometry, as previously indicated. The decrease in the metal-chloride angles may be accredited to intramolecular hydrogen bond.<sup>[16,26]</sup>

## 2.8.9 | Molecular electrostatic potential (MEP)

In order to study the reactions, electrostatic potential  $V(r)$  maps were calculated which are known for the identification of the electronic charge distribution around molecular surface and subsequently to forecast sites for the reactions. These maps were calculated by using the same basis set as for optimization. In the present study, 3D plots of MEP were drawn from the ligand and its Cu (II) complex. Based on the MEP, one can generally order the electron-rich area which has red colour on the map (favour site for electrophilic attack). However, the electron-poor region has a blue color (favour site for nucleophilic attack). But the region with green colour points to the neutral electrostatic potential region. It can be seen that the H<sub>2</sub>L is stable having a very nearly uniform distribution of charge density. However, oxygen and nitrogen atoms are surrounded by a greater negative charge surface, making these sites potentially more

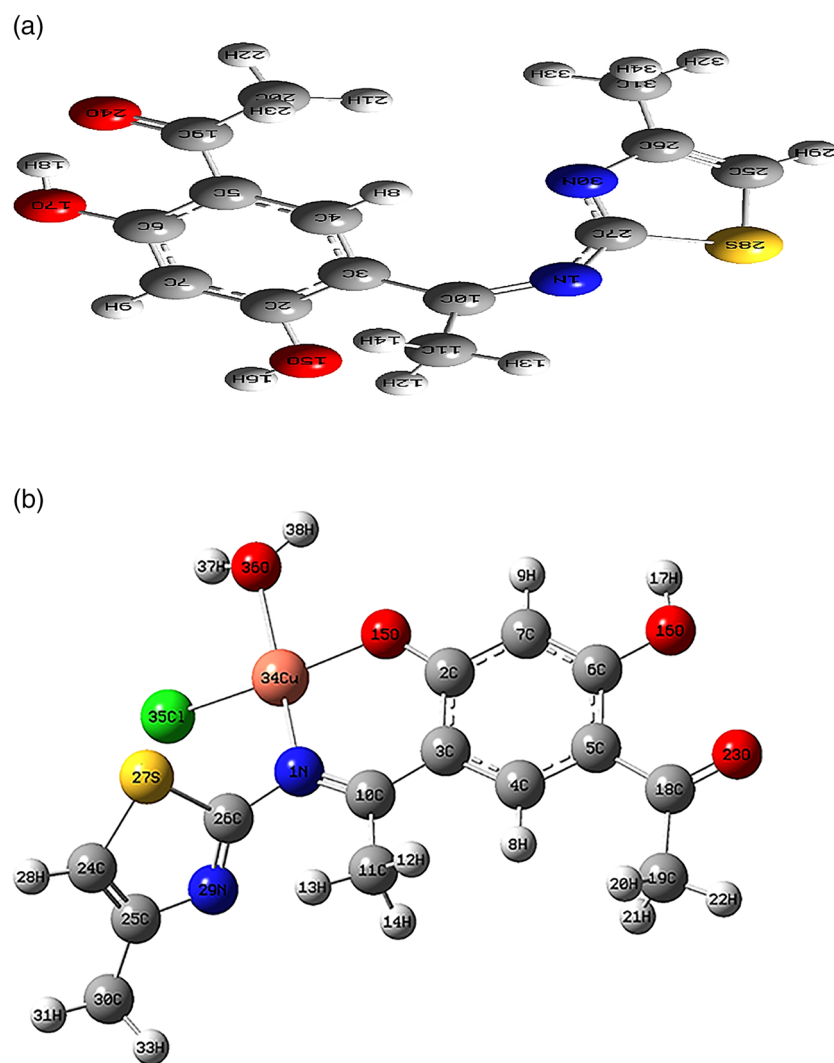


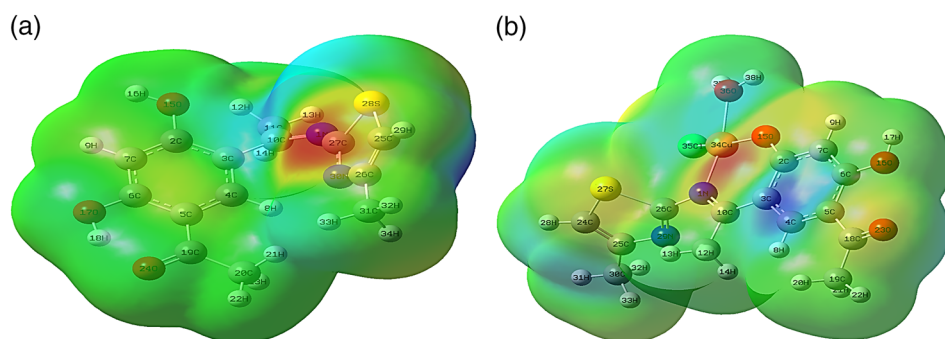
**FIGURE 3** The optimized structures of (a) H<sub>2</sub>L and (b) [Cu (HL)Cl(H<sub>2</sub>O)]H<sub>2</sub>O complex

**TABLE 2** The different optimized and quantum chemical parameters of H<sub>2</sub>L and its Cu (II) complex

Bond lengths (Å)	H <sub>2</sub> L	[Cu (HL) Cl(H <sub>2</sub> O)]H <sub>2</sub> O
C(10)-N(1)	1.30	1.34
O(15)-C(2)	1.39	1.33
C(27)-N(1) in ligand which renumbered as C(26)-N(1) in Cu (II) complex	1.38	1.42
O(15)-H(16)	0.98	
Cu(34)-O(15)		1.92
Cu(34)-N(1)		1.99
Cu(34)-Cl(35)		2.31
Cu(34)-O(36)		2.00
<b>Bond angles (°)</b>		
O(36)-Cu(34)-Cl(35)		84.50
O(36)-Cu(34)-O(15)		84.34
N(1)-Cu(34)-O(15)		92.5
N(1)-Cu(34)-Cl(35)		103.26
<b>The calculated quantum chemical parameters</b>		
E (a.u.)	-887.05	-1174.06
Dipole moment (Debye)	1.01	2.43
E <sub>HOMO</sub> (eV)	-6.26	-6.53
E <sub>LUMO</sub> (eV)	-2.18	-3.81
Δ E (eV)	4.08	2.45
χ (eV)	-4.22	-5.17
η (eV)	2.04	1.23
σ (eV) <sup>-1</sup>	0.49	0.82
Pi (eV)	4.22	5.17
S (eV) <sup>-1</sup>	0.25	0.41
ω (eV)	4.36	10.87
ΔN <sub>max</sub>	-2.07	-4.20

propitious for electrophilic attack (red) as shown in Figure 4.<sup>[16]</sup>

The aromatic ring appeared neutral in terms of electron density. Thus the distribution of potential is in

**FIGURE 4** Molecular electrostatic potential maps of (a) H<sub>2</sub>L and (b) [Cu (HL)Cl(H<sub>2</sub>O)]H<sub>2</sub>O complex. The electron density isosurface is 0.004 a.u

favour of the complexation reaction which is further confirmed by the electrostatic potential distribution of Cu (II) complex, where a greater negative charge is surrounded to the metal centre (Figure 4b). The Mulliken electronegativity also indicated the increase of electronegativity of oxygen and nitrogen in Cu (II) complex than free H<sub>2</sub>L making them the favour site of electrophilic attack by metal ion.<sup>[16,26]</sup>

### 2.8.10 | Molecular parameters

Additional parameters such as the highest occupied molecular orbital energy (E<sub>HOMO</sub>), the lowest unoccupied molecular orbital energy (E<sub>LUMO</sub>), ΔE, absolute electronegativities, χ, chemical potentials, Pi, absolute hardness, η, absolute softness, σ, global electrophilicity, ω, global softness, S, and additional electronic charge, ΔN<sub>max</sub> have been estimated for the H<sub>2</sub>L free ligand and its Cu (II) complex and registered in Table 2. Electrophilicity index (ω) is one of the most essential quantum chemical descriptors in describing reactivity and the toxicity of various specific sites. The electrophilicity may quantify the biological activity of drug receptor interaction. Also, this index measures the stabilization energy when the system acquires an extra negative charge from the environment. η and σ indexes, are the measure of the molecular stability and reactivity also, their concepts are related to each other. The softness indexes are the vice versa image for global hardness. These parameters are useful in order to support the suggestion structures. The mentioned quantum chemical parameters were calculated with the help of the following equations:

$$\Delta E = E_{LUMO} - E_{HOMO} \quad (1)$$

$$\chi = -(E_{HOMO} + E_{LUMO})/2 \quad (2)$$

$$\eta = (E_{LUMO} - E_{HOMO})/2 \quad (3)$$

$$\sigma = 1/\eta \quad (4)$$

$$Pi = -\chi \quad (5)$$

$$S = 1/2\eta \quad (6)$$

$$\omega = Pi/2\eta \quad (7)$$

$$\Delta N_{max} = Pi/\eta \quad (1)$$

The data calculated were presented in Table 2 and reflected the following notes:

- i. The data of H<sub>2</sub>L and its Cu (II) complex had a great chance and priority for biological activity based on high  $\omega$  value.
- ii. S and  $\omega$  were the softness indexes while  $\eta$  is for hardness indication; a hard molecule had a high stability due to its high energy difference in-between the E<sub>HOMO</sub> and E<sub>LUMO</sub> than the soft molecule. So, the soft molecule was the reactive one having flexible donation towards the metal ions. Accordingly, the investigated H<sub>2</sub>L molecule was soft towards the coordination.
- iii. The positive electrophilicity index ( $\chi$ ) value and the negative electronic, chemical potential ( $\mu$ ) value indicated that the H<sub>2</sub>L molecule capable of accepting electrons from the environment and its energy must decrease upon accepting electronic charge. Therefore, the electronic, chemical potential must be negative.
- iv. The Cu (II) complex showed high values of dipole moments than the free ligand.

Both the highest occupied molecular orbital (HOMO) and lowest unoccupied molecular orbital (LUMO) were the main orbitals that participate in chemical stability. The HOMO represents the ability to donate an electron, LUMO as an electron acceptor represents the ability to obtain an electron. From the attained data (Table 2), it can assume that:

1. The energies of the HOMO and LUMO were negative values and more negative than free H<sub>2</sub>L, which showed the stability of isolated complex.
2. The E<sub>HOMO</sub> and E<sub>LUMO</sub> values of Cu (II) complex were calculated and showed a decrease than the free ligand which represents the strength of M–HL shorter bonds.
3. The total energy of Cu (II) complex was higher than free ligand, which indicated greatly the stability of the isolated solid complex.
4. The small energy gap can be associated with a high chemical reactivity, low kinetic stability and reflects to efficient electronic charge transfer interaction making the molecule highly polarizable.
5. The HOMO level was mostly localized on the azomethine nitrogen and oxygen of the phenol group in the ligand, which indicated the preferable sites for nucleophilic attack to the central metal atom.<sup>[16,27]</sup>

### 2.8.11 | UV-vis spectra

An identification of the photochemistry of transition metal compounds needs knowledge of the properties of molecular orbitals and appropriate excited states. Frontier orbitals played a pertinent role in such systems,

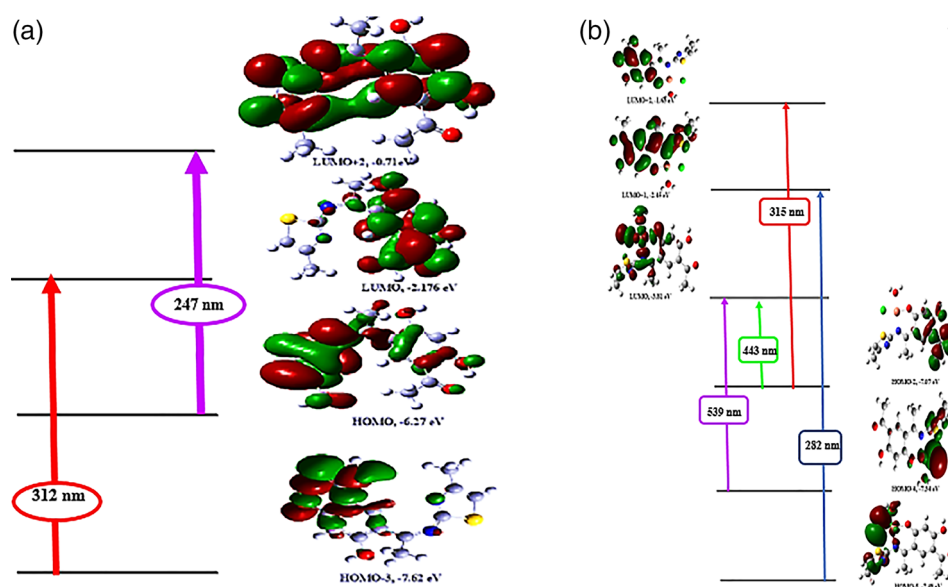


**FIGURE 5** a Theoretical electronic absorption transitions for H<sub>2</sub>L in ethanol solvent. b Theoretical electronic absorption transitions for [Cu (HL)Cl(H<sub>2</sub>O)] H<sub>2</sub>O complex in DMF solvent

**TABLE 3** Main calculated optical transition with composite ion in terms of molecular orbitals

Compound	Transition	Excitation energy (ev)	$\lambda_{\max}$ Calc. (nm)	$\lambda_{\max}$ exp. (nm)	Oscillating strength
H <sub>2</sub> L	HOMO-3 $\longrightarrow$ LUMO	3.98	312	321	0.003
	HOMO $\longrightarrow$ LUMO+2	5.03	247	248	0.080
[Cu(HL)Cl (H <sub>2</sub> O)]H <sub>2</sub> O	HOMO-4 $\longrightarrow$ LUMO	2.30	539	537	0.010
	HOMO-2 $\longrightarrow$ LUMO	2.80	443	446	0.001
	HOMO-2 $\longrightarrow$ LUMO+2	3.94	315	319	0.001 $\times 10^{-1}$
	HOMO-5 $\longrightarrow$ LUMO+1	4.39	282	252	0.013
	-----	-----	----	226	-----

because they rule the electronic excitations and the transition characters. With the aid of TD-DFT calculations, it is possible to have comments on the contributions of the ligand and metal orbitals to molecular orbitals. It is not practical to analyse all the electronic transitions and the orbitals; therefore some limits were used. Because it is high accuracy and low computational cost of TD-DFT, it

has been popularized for theoretical inspection of electronic spectra of molecules. The present inspection of low lying excited state of optimized ground state structures of H<sub>2</sub>L and its Cu (II) complex has been performed at TD-DFT/B3LYP/LANL2DZ level of theory for 30 singlet state. In Table 5, the experimental and theoretical electronic spectra were presented. The TD-DFT calculations

**TABLE 4** Biological activity of Schiff base ligand and metal complexes

Sample	Inhibition zone diameter (mm/mg sample)			
	(Gram positive)		(Gram negative)	
	<i>bacillus subtilis</i>	<i>Staphylococcus aureus</i>	<i>Escherichia coli</i>	<i>Pseudomonas aeruginosa</i>
Control: DMSO	0	0	0	0
ligand (H <sub>2</sub> L)	11 $\pm$ 0.041	0	0	0
[Cr (HL)(H <sub>2</sub> O) <sub>3</sub> Cl]Cl <sub>2</sub> .4H <sub>2</sub> O	11 $\pm$ 0.031	12 $\pm$ 0.027	13 $\pm$ 0.041	13 $\pm$ 0.033
[Mn (HL)(H <sub>2</sub> O) <sub>4</sub> ]Cl <sub>2</sub> .2H <sub>2</sub> O	12 $\pm$ 0.035	14 $\pm$ 0.024	11 $\pm$ 0.027	12 $\pm$ 0.031
[Fe (HL)(H <sub>2</sub> O) <sub>4</sub> ]Cl <sub>2</sub> .H <sub>2</sub> O	17 $\pm$ 0.026	15 $\pm$ 0.041	16 $\pm$ 0.030	15 $\pm$ 0.026
[Co (HL)(H <sub>2</sub> O) <sub>4</sub> ]Cl <sub>2</sub> .5H <sub>2</sub> O	25 $\pm$ 0.033	20 $\pm$ 0.018	24 $\pm$ 0.026	21 $\pm$ 0.028
[Ni (HL)(H <sub>2</sub> O) <sub>4</sub> ]Cl <sub>2</sub> .3H <sub>2</sub> O	20 $\pm$ 0.019	15 $\pm$ 0.018	15 $\pm$ 0.022	16 $\pm$ 0.024
[Cu (HL)(H <sub>2</sub> O)Cl].H <sub>2</sub> O	24 $\pm$ 0.016	16 $\pm$ 0.019	30 $\pm$ 0.031	21 $\pm$ 0.030
[Zn (HL)(H <sub>2</sub> O) <sub>3</sub> Cl].3H <sub>2</sub> O	16 $\pm$ 0.018	16 $\pm$ 0.021	14 $\pm$ 0.022	15 $\pm$ 0.022
[Cd (HL)(H <sub>2</sub> O) <sub>3</sub> Cl]	24 $\pm$ 0.029	16 $\pm$ 0.022	17 $\pm$ 0.024	25 $\pm$ 0.026
Amikacin	10 $\pm$ 0.032	9 $\pm$ 0.035	6 $\pm$ 0.029	10 $\pm$ 0.027

**TABLE 5** Anti-breast cancer activity of Schiff base ligand (H<sub>2</sub>L) and its metal complexes

Complex	Concn. (µg/ml)	Surviving fraction (MCF7)					IC <sub>50</sub> (µg/ml)
		0.0	5.0	12.5	25.0	50.0	
Ligand H <sub>2</sub> L		1	0.686	0.557	0.271	0.271	15
[Mn (HL)(H <sub>2</sub> O) <sub>4</sub> ]Cl.2H <sub>2</sub> O		1	1.048	0.929	0.757	0.748	-----
[Co (HL)(H <sub>2</sub> O) <sub>4</sub> ]Cl.5H <sub>2</sub> O		1	1.048	0.952	0.729	0.586	-----
[Ni (HL)(H <sub>2</sub> O) <sub>4</sub> ]Cl.3H <sub>2</sub> O		1	0.81	0.762	0.524	0.429	32
[Cu (HL)Cl(H <sub>2</sub> O)]H <sub>2</sub> O		1	0.952	0.867	0.714	0.700	-----
[Zn (HL)(H <sub>2</sub> O) <sub>3</sub> Cl]3H <sub>2</sub> O		1	1.000	0.943	0.762	0.600	-----
[Cd (HL)(H <sub>2</sub> O) <sub>3</sub> Cl]		1	0.852	0.786	0.571	0.410	36

**TABLE 6** Energy values obtained in docking calculations of H<sub>2</sub>L and its metal complexes with Crystal Structure of Human Astrovirus capsid protein (5ibv) receptor

Compound	moiety	Receptor site	Interaction	Distance (Å°)	E (kcal/mol)
Ligand (H <sub>2</sub> L)	S28	O THR 329	H-donor	3.49	-0.5
	O24	NZ LYS 273	H-acceptor	3.11	-5.4
	N1	OE1 GLU 103	ionic	3.78	-1.0
	5-ring	CA GLY 93	pi-H	4.11	-2.1
	6-ring	CG2 THR 401	pi-H	4.45	-0.8
[Cr (HL)(H <sub>2</sub> O) <sub>3</sub> Cl] Cl.4H <sub>2</sub> O	S27	OE1 GLU 335	H-donor	3.43	-1.2
	O39	OG SER 332	H-donor	2.91	-9.3
	N1	OE1 GLU 335	ionic	3.08	-4.0
	O35	OE1 GLU 335	ionic	3.65	-1.4
	O39	OE1 GLU 335	ionic	2.32	-11.0
	O42	OE1 GLU 335	ionic	3.36	-2.5
[Mn (HL)(H <sub>2</sub> O) <sub>4</sub> ] Cl.2H <sub>2</sub> O	O15	OD1 ASN 261	H-donor	2.57	-4.2
	O36	OD2 ASP 213	H-donor	3.05	-9.4
	O36	OD1 ASP 213	ionic	2.72	-6.6
	O36	OD2 ASP 213	ionic	3.05	-4.2
[Fe (HL)(H <sub>2</sub> O) <sub>4</sub> ] Cl <sub>2</sub> .H <sub>2</sub> O	O16	OD1 ASN 261	H-donor	2.57	-3.8
	O41	OD1 ASP 213	H-donor	2.62	-17.2
	O41	OD2 ASP 213	H-donor	2.78	-9.5
	O44	OD1 ASP 213	H-donor	3.27	-0.8
	O34	OD1 ASP 213	ionic	3.57	-1.6
	O41	OD1 ASP 213	ionic	2.62	-7.5
	O41	OD2 ASP 213	ionic	2.78	-6.1
	O44	OD1 ASP 213	ionic	3.27	-2.9
	O44	OD2 ASP 213	ionic	3.54	-1.7
	[Co (HL)(H <sub>2</sub> O) <sub>4</sub> ]Cl.5H <sub>2</sub> O	O37	OD1ASP 213	H-donor	3.4
O37		OD2 ASP 213	H-donor	2.77	-25.2
O40		OD1 ASP213	H-donor	2.95	-19.1
O33		OD1 ASP213	ionic	3.89	-0.7

(Continues)

TABLE 6 (Continued)

Compound	moiety	Receptor site	Interaction	Distance (Å <sup>o</sup> )	E (kcal/mol)
	O33	OD2 ASP213	ionic	3.56	-1.7
	O37	OD1 ASP213	ionic	3.4	-2.3
	O37	OD2 ASP213	ionic	2.77	-6.2
	O40	OD1 ASP213	ionic	2.95	-4.8
	O40	OD2 ASP213	ionic	3.83	-0.9
[Ni (HL)(H <sub>2</sub> O) <sub>4</sub> ]Cl.3H <sub>2</sub> O	O33	OD1 ASP 213	H-donor	2.72	-15.7
	O42	OD2 ASP 213	H-donor	3	-10.1
	O33	OD1 ASP 213	ionic	2.72	-6.6
	O33	OD2 ASP 213	ionic	3.65	-1.4
	O39	OD1 ASP 213	ionic	2.78	-6.2
	O39	OD2 ASP 213	ionic	3.46	-2
	O42	OD1 ASP 213	ionic	3.57	-1.6
	O42	OD2 ASP 213	ionic	3	-4.5
[Cu (HL)Cl(H <sub>2</sub> O)] H <sub>2</sub> O	S27	O THR 100	H-donor	3.67	-1.8
	O36	OE1 GLU 335	H-donor	2.64	-27.1
	O36	OE1 GLU 335	ionic	2.64	-7.4
[Zn (HL)Cl(H <sub>2</sub> O) <sub>3</sub> ] 3H <sub>2</sub> O	O16	OD1 ASN 261	H-donor	2.56	-3.4
	O35	OD1 ASP 213	H-donor	2.78	-4.6
	O35	OD2 ASP 213	H-donor	2.91	-12.3
	O35	OD1 ASP 213	ionic	2.78	-6.1
	O35	OD2 ASP 213	ionic	2.91	-5.1
[Cd (HL)(H <sub>2</sub> O) <sub>3</sub> ]Cl	O16	O TYR 132	H-donor	2.82	-2.8
	O41	OD2 ASP 213	H-donor	3.05	-17.8
	O38	OD2 ASP 213	ionic	3.84	-0.9
	O41	OD2 ASP 213	ionic	3.05	-4.2

have been evaluated in the N,N-dimethylformamide solvent background and competed with the experimental data. The transitions between interfrontier orbitals for wavelengths corresponding to the maximum oscillator strength of simulated results with recent experimental observations were presented in Figure (5 a, b). For example, the electronic transitions for H<sub>2</sub>L obtained at calculated 247 nm correspond to experimental peak at 248 nm. This transition have been majorly contributed from HOMO to LUMO+2 transitions which was primarily  $\pi \rightarrow \pi^*$  in nature. The different transitions and its experimental counterpart of the free ligand and its Cu (II) complex have been reviewed in Table 3.<sup>[26]</sup>

### 2.8.12 | Structural interpretation

Theoretical approaches made by Liang and Lipscomb indicated that the nitrogen atom was more negatively

charged than the oxygen atom in the isolated metal ion and so it may account for the coordination of the nitrogen atom instead of the oxygen atom, to the metal ion. Furthermore, these authors have found that in the presence of the metal ions, the bidentate binding conformation with both N and O atoms coordinated to the metal ions was favoured.

The structures of the Schiff base ligand (H<sub>2</sub>L) with Cr (III), Mn (II), Fe (III), Co (II), Ni (II), Cu (II), Zn (II) and Cd (II) complexes were characterized via elemental analyses, molar conductance, magnetic, solid reflectance and thermal analysis data and the proposed structures of metal complexes were reported in Figure 6.

### 2.8.13 | Biological activity

The greater antibacterial activity of metal complexes than the free Schiff base ligands can be justified by chelation

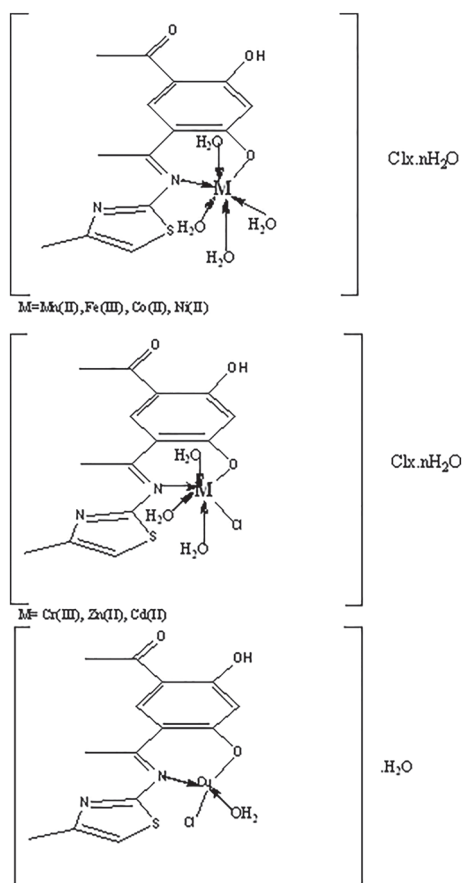


FIGURE 6 Structures of metal complexes

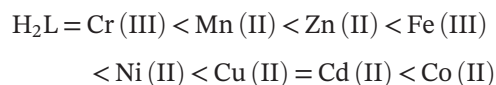
of the Schiff base with metal ions as metal chelates display both nonpolar and polar properties. This makes them suitable for permeation into cells and tissues. The polarity of the metal ion will be decrease to a greater extent due to the overlap of the ligand orbital upon chelation, and partial sharing of the positive charge of the

metal ion with donor groups. Chelation increased the delocalization of  $\pi$ -electrons over the entire chelate ring and enhanced the penetration of the complexes into lipid membranes. It also increased the hydrophobic and lipophilic nature of the central metal ions, perhaps leading to liposolubility and permeability through the lipid layer of cell membranes. Further, lipophilicity, which controls the rate of entry of molecules into the cell, was modified by coordination, so the metal complex can become more active than the free Schiff base ligand.<sup>[16,26]</sup>

Schiff base ligand and its complexes were screened for antibacterial activities. The results listed in Table (4) and Figure 7 showed that complexes exhibited more inhibitory effects than the parent ligand.

Antibacterial activity of H<sub>2</sub>L ligand and Cr (III), Mn (II), Fe (III), Co (II), Ni (II), Cu (II), Zn (II) and Cd (II) complexes were tested against various bacterial species: two Gram (+) *Staphylococcus aureus* and *Bacillus subtilis* and two Gram (-) *pseudomonas aeruginosa* and *Escherichia coli* by using the modified agar diffusion method.

For *Bacillus subtilis*: the biological activity follows the order:



For *Staphylococcus aureus*: the Co (II) complex showed the highest activity. The activity follows the order:

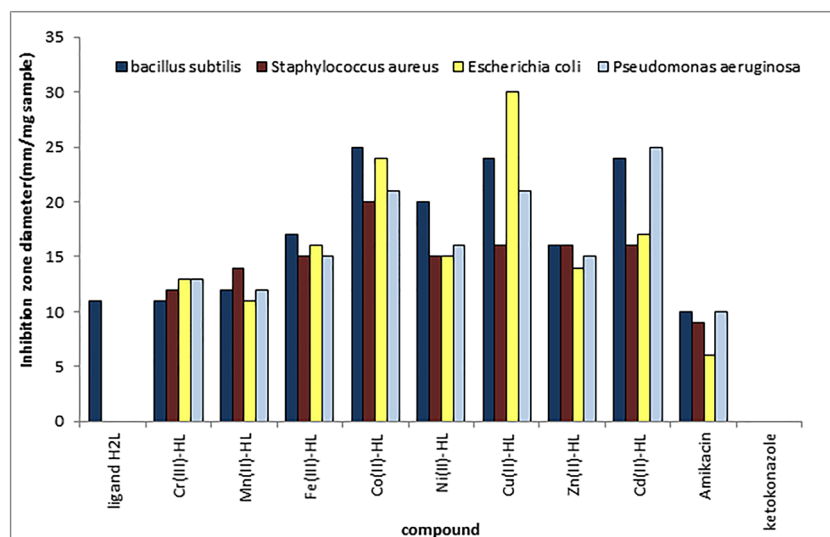
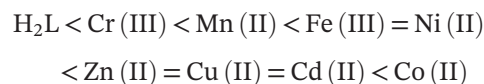
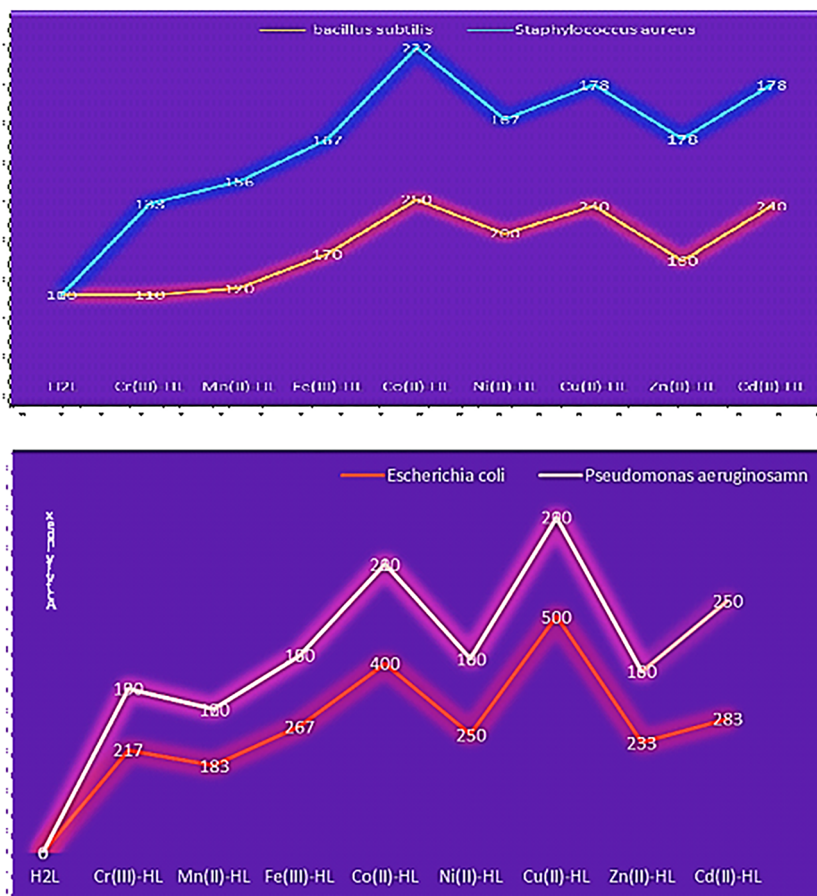
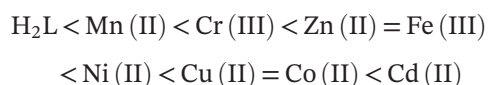


FIGURE 7 Biological activity of Schiff base ligand and its metal complexes against different organisms

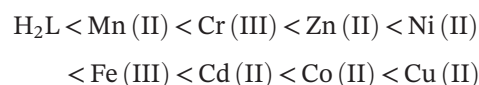
**FIGURE 8** Activity index values of H<sub>2</sub>L and its metal complexes



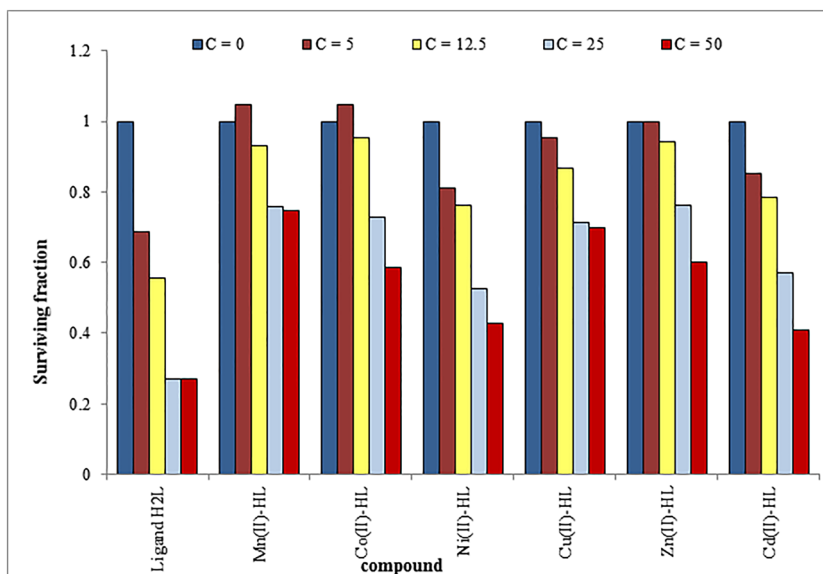
For *pseudomonas aeruginosa*: the biological activity follow the order:



For *Escherichia coli*: the biological activity follow the order:



**FIGURE 9** Anticancer activity of Schiff base ligand (H<sub>2</sub>L) and its metal complexes



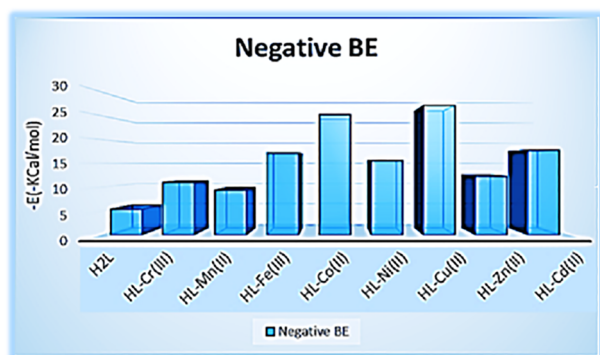


**FIGURE 10** The relation between the negative lowest binding energy of the ligand and its metal complexes with 5IBV receptor

The activities of the prepared Schiff base ligand and its metal complexes were confirmed via calculating the activity index according to the following relation and that showed in Figure 8.<sup>[27]</sup>

$$\text{Activity index (A)} = \frac{\text{Inhibition Zone of compound (mm)}}{\text{Inhibition Zone of standard drug (mm)}} \times 100.$$

It can be conducted from this arrangement that the antimicrobial activity of the complexes is greater than related ligand. The increased activity of the metal complexes can be rationalized on the basis of chelation theory.<sup>[15]</sup> Chelation decreases the polarity of the metal ion, because positive charges of the metal are partially shared with the donor atoms extent in the ligands and there may be  $\pi$ -electron delocalization over the whole chelation. This phenomenon improved the lipophilic character of the metal chelate and favours its permeation more efficiently through the lipid layer of the microorganism. As the results of antimicrobial activity is related to their ability to make complexes with soluble extracellular proteins and with the cell wall, for the lipophilic character of these compounds, which may bring about the rupture of the cell membrane of microorganisms. In addition, in bacteria, the permeability of the cell membrane is associated with the loss of ions as well as the decrease

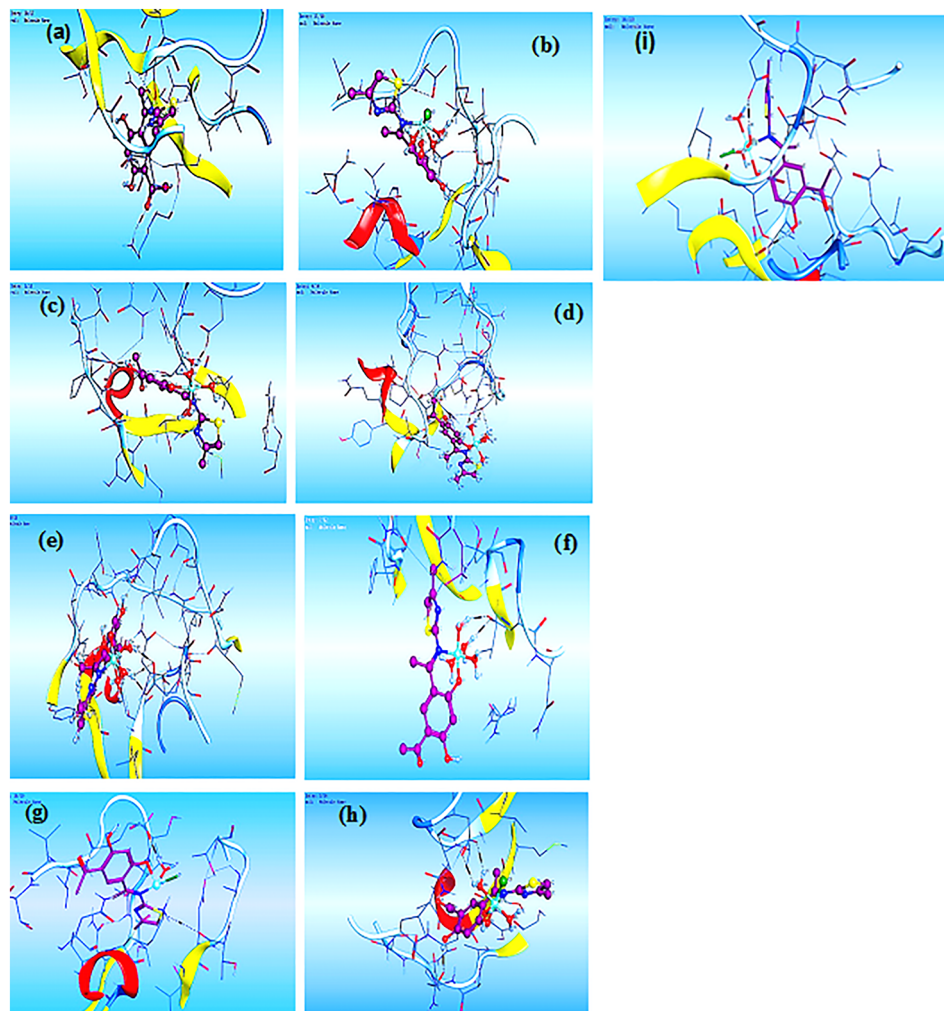


**FIGURE 11** The interaction between H<sub>2</sub>L and its metal complexes with receptor 5IBV. (a) H<sub>2</sub>L, (b) Cr (III), (c) Mn (II), (d) Fe (III), (e) Co (II), (f) Ni (II), (g) Cu (II), (h) Zn (II) and (i) Cd (II) complexes

of its potential, causing damage that may lead to the extravasation of macromolecules, resulting in a collapse of the cellular functions and, consequently, the bacterial death.<sup>[15]</sup>

### 2.8.14 | Anticancer activity

Metal-based anticancer drug discovery is one of the future areas of pharmaceutical research. The ligand and its complexes were investigated for their anticancer activity against human breast cancer cell line MCF-7 via using 100 µg/ml concentration. It is apparent that Cr (III), Mn (II), Ni (II), Zn (II) and Cd (II) complexes and H<sub>2</sub>L ligand were found to be very active against breast cancer cells. Table (5) and Figure 9 showed the effect of various concentrations i.e. (0, 5, 12, 25 and 50 µg/ml of each one) of testing compounds on human breast cancer cell line MCF-7. The IC<sub>50</sub> (the concentration of the compound in µg/ml that inhibits proliferation of the cells by 50% as compared to the untreated control cells) values of the investigated compounds were listed in Table (5). The ligand showed IC<sub>50</sub> values of 15.00 µg/ml towards human breast cancer cell lines (MCF-7), while the Ni (II) and Cd (II) complexes were also exhibited good anticancer activity with IC<sub>50</sub> values of 32.00 and 36.00 µg/ml, respectively. The ligand was prepared and then showed high activity on the cancer cells and followed the rules with preparation metal complexes to know how effective they are, but because cancer cells are not like normal cells, it could be argued that the rules used to guide the design of metal-based drugs are entirely valid and should be followed, since the drugs that have made it into the clinic to date follow these rules. However, there are numerous examples of compounds which have been studied on advanced pre-clinical models or are currently undergoing clinical trials, e.g. the arsenic–glutathione prodrugs that target certain tumours as well as others described previously.<sup>[24]</sup> There is clearly a long way to go before saying that certain classes of metal complexes should be excluded from medicinal inorganic chemistry and a better understanding of biology and the use of assays other than cytotoxicity screening are essential to guide metal-based drug design in the future.<sup>[28]</sup>

### 2.8.15 | Molecular modelling: Docking study

Molecular docking studies have been carried out in order to predict the binding modes of the H<sub>2</sub>L ligand and its metal complexes to Crystal Structure of Human

Astrovirus capsid protein (5IBV). Human astrovirus (HAsV) is a leading cause of viral diarrhoea in infants and young children worldwide. HAsV is a non-enveloped virus with a  $T = 3$  capsid and a positive-sense RNA genome. The lowest binding energies of the ligand and its metal complexes by 5IBV receptor were calculated and showed in Figure 10. 3D interaction maps showed the binding models of H<sub>2</sub>L and its metal complexes to the Human astrovirus RNA. It was found that all of the tested compounds were interacted with the RNA through a hydrogen bond and a  $\pi$  interaction (Table 6) and Figure 11. The values of interaction energies revealed that its Cu (II) complex had the most stable interaction.<sup>[28,29]</sup>

## 3 | CONCLUSION

The novel complexes of chromium (III), manganese (II), iron (III), copper (II), nickel (II), cobalt (II), zinc (II) and cadmium (II) with the bidentate ligand (H<sub>2</sub>L) were synthesized by condensation off 4,6-diacetylresorcinol with 2-amino-4-methylthiazole and characterized using spectroscopic methods. From the data of elemental analysis, the complexes had composition of the MHL type with general formulae [M (HL)(H<sub>2</sub>O)<sub>4</sub>]Cl<sub>x</sub>.nH<sub>2</sub>O (M = Mn (II),  $x = 1$ ,  $n = 2$ ; Fe (III),  $x = 2$ ,  $n = 1$ ); Co (II),  $x = 1$ ,  $n = 5$ ; and Ni (II),  $x = 1$ ,  $n = 3$ ) and [M (HL)(H<sub>2</sub>O)<sub>3</sub>Cl]Cl<sub>x</sub>.nH<sub>2</sub>O (M = Cr (III),  $x = 1$ ,  $n = 4$ ; Zn (II),  $x = 0$ ,  $n = 3$ ; and Cd (II)  $x = 0$ ,  $n = 0$ ), [Cu (HL)(H<sub>2</sub>O)Cl]H<sub>2</sub>O. The ligand acted as neutral bidentate (NO) ligand and all complexes showed octahedral geometry except Cu (II) showed tetrahedral geometry. The molar conductivity data for complexes indicated that Cu (II), Zn (II) and Cd (II) complexes were considered as nonelectrolytes. Cr (III), Mn (II), Co (II) and Ni (II) complexes are ionic in nature and they are 1:1 electrolytes. The Fe (III) complex was a 1:2 electrolyte. The antimicrobial test referred that some complexes had higher antimicrobial activity in comparison with that of the free Schiff base ligand. In addition to that, cytotoxicity of Cd (II) complex indicated higher anticancer activity than the others with IC<sub>50</sub> 32 µg/ml that might become a good anticancer agent in clinical trials or biological agents. The docking study showed that the Cu (II) complex has the highest activity with lowest binding energy ( $-27.1$  kcal mol<sup>-1</sup>) with Human Astrovirus capsid protein.

### ORCID

Walaa H. Mahmoud  <https://orcid.org/0000-0001-9187-4325>

Gehad G. Mohamed  <https://orcid.org/0000-0002-1525-5271>

## REFERENCES

- [1] W. H. Mahmoud, R. G. Deghadi, G. G. Mohamed, *Appl. Organomet. Chem* **November 2017**, 2018, 1.
- [2] S. Ahmadian-fard-fini, M. Salavati-niasari, F. Mohandes, *Bull. Mater. Sci* **2014**, 37, 753.
- [3] S. M. Al-Barody, H. Ahmad, *Cogent Chem* **2015**, 1, 1.
- [4] D. Nasrin, M. A. Alam, I. M. M. Rahman, H. Banu, M. Nazimuddin, *Int J Appl Nat Sci* **2013**, 2, 1.
- [5] A. W. Bauer, W. M. Kirby, C. Sherris, M. Turck, *Am. J. Clin. Pathol.* **1966**, 45, 493.
- [6] L. D. Liebowitz, H. R. Ashbee, E. G. V. Evans, Y. Chong, N. Mallatova, M. Zaidi, D. Gibbs, *Diagnostic Microbiology and Infectious Disease* **2001**, 4, 27.
- [7] National Committee for Clinical Laboratory Standards. Performance VOL. 41, 1997 antimicrobial susceptibility of Flavobacteria **1993**.
- [8] National Committee for Clinical Laboratory Standards. National Committee for Clinical Laboratory Standards, Villanova, PA. **1993**
- [9] M. J. Matar, L. Ostrosky-Zeichner, V. L. Paetznick, J. R. Rodriguez, E. Chen, J. H. Rex, *Antimicrob. Agents Chemother.* **2003**, 47, 1647.
- [10] W. H. Mahmoud, R. G. Deghadi, G. G. Mohamed, *Appl. Organomet. Chem.* **2016**, 30, 221.
- [11] P. Skehan, R. Storeng, D. Scudiero, A. Monks, J. McMahon, D. Vistica, J. T. Warren, H. Bokesch, S. Kenney, M. R. Boyd, *Journal of the National Cancer Institute* **1990**, 82, 1107.
- [12] W. H. Mahmoud, N. F. Mahmoud, G. G. Mohamed, A. A. El-Bindary, A. Z. El-Sonbati, *J. Mol. Struct.* **2015**, 1086, 266.
- [13] W. H. Mahmoud, N. F. Mahmoud, G. G. Mohamed, *J Therm Anal Calorim* **2017**.
- [14] V. Uivarosi, *J Molecules.* **2013**, 11153.
- [15] E. Yousif, A. Majeed, K. Al-Sammarrae, N. Salih, J. Salimon, B. Abdullah, *Arabian Journal of Chemistry* **2017**, 10, S1639.
- [16] W. H. Mahmoud, G. G. Mohamed, H. A. Elsayy, M. A. Radwan, *Appl. Organomet. Chem* **2018**, 1.
- [17] A. A. Emara, O. M. Adly, *Transition Met. Chem* **2007**, 32, 889.
- [18] M. Shebl, M. A. El-Ghamry, S. M. E. Khalil, M. A. A. Kishk, *Spectrochim Acta - Part a Mol Biomol Spectrosc* **2014**, 126, 232.
- [19] A. Thakar, K. Joshi, K. Pandya, A. Pancholi, *E-Journal of Chemistry* **2011**, 8, 1750.
- [20] A. F. Santos, D. F. Brotto, L. R. V. Favarin, N. A. Cabeza, G. R. Andrade, M. Batistote, A. A. Cavalheiro, A. Neves, D. C. M. Rodrigues, A. dos Anjos, *Brazilian J Pharmacogn.* **2014**, 24, 309.
- [21] K. K. Abid, A. B. Omar, *Res. Chem. Intermed.* **2015**, 41, 1715.
- [22] W. H. Mahmoud, N. F. Mahmoud, G. G. Mohamed, *Appl. Organomet. Chem.* **2016**, 30, 959.
- [23] W. H. Mahmoud, R. G. Deghadi, G. G. Mohamed, *J. Therm. Anal. Calorim.* **2017**, 127, 2149.
- [24] W. M. I. Hassan, M. A. Badawy, G. G. Mohamed, H. Moustafa, S. Elramly, *Spectrochimica Acta a* **2013**, 111, 169.
- [25] K. Dhahagani, M. Kesavan, K. G. G. Vinoth, L. Ravi, G. Rajagopal, J. Rajesh, *Mater. Sci. Eng. C* **2018**, 1(90), 119-130.
- [26] W. H. Mahmoud, G. G. Mohamed, O. Y. El-Sayed, *Appl. Organomet. Chem.* **2017**, 1.
- [27] C. S. Allardyce, P. J. Dyson, *Applied Organometric Chemistry* **2016**, 3201.
- [28] M. Habib, A. Beyramabadi, S. Allameh, M. Khashi, A. Morsali, M. Pordel, C. Khorsandi, *J. Mol. Struct.* **2017**, 1143, 424.
- [29] A. Rauf, A. Shah, K. S. Munawar, S. Ali, M. N. Tahir, M. Javed, A. M. Khan, *Arabian J Chem* **2017**.

**How to cite this article:** Mahmoud WH, Omar MM, Ahmed YM, Mohamed GG. Transition metal complexes of Schiff base ligand based on 4,6-diacetyl resorcinol. *Appl Organometal Chem.* 2020; e5528. <https://doi.org/10.1002/aoc.5528>